Experimental and numerical studies of square concrete-filled double steel tubular short columns under eccentric loading

Ahmed, M., Liang, Q. Q., Patel, V. I. and Hadi, M. N. S. (2019). Experimental and numerical studies of square concrete-filled double steel tubular short columns under eccentric loading. *Engineering Structures*, 197: 109419.

Experimental and numerical studies of square concrete-filled double steel tubular short columns under eccentric loading

Mizan Ahmed[a], Qing Quan Liang[a,1], Vipulkumar Ishvarbhai Patel[b], Muhammad N. S. Hadi[c]

[a] *College of Engineering and Science, Victoria University, PO Box 14428, Melbourne, VIC 8001, Australia*
[b] *School of Engineering and Mathematical Sciences, La Trobe University, Bendigo, VIC 3552, Australia*
[c] *School of Civil, Mining and Environmental Engineering, University of Wollongong, Wollongong, NSW 2522, Australia*

ABSTRACT

Square concrete-filled double steel tubular (CFDST) beam-columns consisting of an internal circular steel tube have increasingly been utilized in composite building structures because of their high structural performance. This paper describes experimental and numerical studies on the structural responses of square thin-walled CFDST columns loaded eccentrically. Tests on twenty short square CFDST columns were undertaken that included sixteen columns under eccentric loading and four columns under concentric loading. The parameters examined in the experiments included the cross-sectional dimensions, the width-to-thickness ratios of outer and internal tubes and loading eccentricity. The measured ultimate strengths, load-shortening responses, load-lateral displacement curves, stress-strain curves and observed failure modes are presented. A numerical model incorporating the fiber analysis is developed that predicts the moment-curvature responses and axial load-moment strength envelopes of CFDST columns. The model explicitly accounts for the influences of the confinement exerted by the internal

[1]Corresponding author.
E-mail address: Qing.Liang@vu.edu.au (Q. Q. Liang)

circular steel tube on the core concrete and the progressive post-local buckling of the external steel tube. Efficient computer algorithms implementing the inverse quadratic method is developed to produce converged solutions to the nonlinear dynamic equilibrium equations generated in the analysis. Measurements from the tests are employed to validate the proposed numerical model. It is shown that there is a good agreement between theory and experiment. The computer model is utilized to demonstrate the significance of various parameters on the behavior of thin-walled short CFDST beam-columns.

Keywords: Concrete-filled double steel tubes; Local and post-local buckling; Nonlinear analysis.

1. Introduction

Square concrete-filled double steel tubular (CFDST) columns as depicted in Fig. 1 are used in composite building structures due to their aesthetic appearance and ease of connecting with steel beams in addition to their high structural and fire performance. The external steel tube of a CFDST square column is fabricated by thin-walled section to decrease the usage of steel material for economical designs. However, this may cause the outward local buckling of the steel tube under compression, which has a marked influence on the performance of CFDST columns and should be considered in the nonlinear analysis and design. The internal circular steel tube effectively confines the core-concrete in a loaded CFDST column, which remarkably improves the concrete compressive strength as well as ductility. The CFDST columns in a building structure are likely subjected to eccentric loading or the combination of bending and axial load, and are designed as beam-columns. Little research has been reported on the structural behavior of thin-walled CFDST square columns that are subjected to eccentric loads. This paper

presents experimental and numerical investigations on the behavior of CFDST columns loaded eccentrically to failure.

Most of the investigations on CFDST columns reported previously has focused on circular cross-section [1-12] and tests on short square CFDST columns consisting of an inner circular steel tube have been very limited [13-16]. Pei [13] performed tests to determine the structural performance of stub CFDST square columns under axial and eccentric loads. It was reported that the local buckling of the external steel tube in addition to concrete crushing caused the failure of short CFDST square columns. Experiments on the structural behavior of square CFDST short columns loaded either concentrically or eccentrically to failure were undertaken by Qian et al. [14, 15] . The failure of the columns was due to the bending as well as the outward local buckling of the outer steel tube. Since the internal circular tube confined the core concrete, the residual ductility and strength of CFDST columns were dramatically improved. Recently, Wang et al. [16] presented experimental investigations on the characteristics of axially-loaded short square CFDST columns incorporating stiffeners. It was reported that all CFDST columns failed by the outward local-buckling of the outer steel tube walls at the stiffeners coupled with stiffener buckling as well as sandwiched concrete crushing.

Commercial finite element (FE) programs have been employed to model the structural behavior of square CFDST stub columns loaded concentrically to failure by investigators. Pei [13] presented FE models created by using the FE program ANSYS for ascertaining the load-axial strain behavior of short CFDST square columns. The core-concrete was modeled by the stress-strain relations presented by Zhong [17] for concrete confined by circular steel tubes while the sandwiched-concrete was simulated by the material constitutive laws given by Han [18] for concrete in square CFST columns. However, the FE models by Pei [13] did not include the

local buckling of the outer steel tube as well as the composite action between the concrete and steel components so that they overestimated the experimentally measured behavior of CFDST columns. Qian et al. [14] utilized the FE software ABAQUS to model the responses of a short square CFDST column loaded concentrically to failure. The nonlinear analysis employed the constitutive model given by Han [18] for sandwiched concrete and the relationship of stress and strain given by Sun and Kenji [19] for core concrete. The FE model presented by Qian et al. [14], which considered the local buckling of the outer steel tube, was shown to predict well the behavior of the concentrically loaded CFDST column. Wang et al. [16] utilized ABAQUS to investigate the interaction behavior of concrete and steel tube in axially loaded stub CFDST columns with outer square sections. The concrete model developed by Tao et al. [20] was adopted for both sandwiched and core concrete. However, the local buckling of the external tube was not included in the modeling.

The effects of local buckling on the structural performance of concrete-filled steel tubular composite columns have been investigated by a number of researchers [21-28]. A fiber-based modeling technique has been proposed by Ky et al. [29] for the response predictions of axially loaded concrete-encased composite (CEC) short and slender columns. The modeling technique, which took into account the local buckling of structural steel, buckling of reinforcement bars, initial geometric imperfection and concrete confinement, was shown to capture well the behavior of CEC columns. Liu et al. [30] developed a numerical model for the inelastic analysis of nonlinear steel–concrete composite beams curved in-plan. However, very limited experimental and numerical research works have been conducted on the performance of short CFDST square beam-columns. Moreover, no fiber-based computational technique has been proposed for the simulation of the moment-curvature curves and interaction strengths of such beam-columns. To fill this knowledge gap, this paper presents experimental and numerical

studies on the structural performance of CFDST square stub columns loaded eccentrically. A total of twenty short columns with different loading eccentricities were tested to failure to examine their structural responses. The experimental program and results obtained are described. A mathematical modeling method for the prediction of the moment-curvature curves and strength envelopes of CFDST beam-columns is developed and validated against test data. The computational model is then utilized to assess the impacts of important design parameters on the structural behavior of short CFDST square beam-columns.

2. Experimental program

2.1. Specimen preparation

Twenty short square CFDST columns fabricated by square outer steel tubes and circular inner steel tubes were tested to failure under either eccentric or concentric loading. The specimens were divided into four groups (G1, G2, G3 and G4). There were five specimens in each group. For Groups G1 and G3, the specimens had an external square cross-section of 125×125 mm and an inner circular tube with a diameter of 76.1 mm. Specimens in Groups G2 and G4 had an outer square cross-section of 150×150 mm and an inner circular tube with a diameter of 88.9 mm. The thickness of the inner steel tubes was varied to investigate their effects on the structural performance. The column specimens were originally designed to be tested using the compression testing machine with a capacity of 2000 kN at Victoria University, Australia. The maximum size of the column specimens that could be tested using this machine was 150×150 mm. For CFDST columns, the cross-section smaller than 125×125 mm was too small to place the inner tube and concrete. The specimens were fabricated by cold-formed steel tubes, which were placed concentrically and welded with two steel bars. Two stiffeners were welded on each

face of the ends of the steel square tube to prevent the premature failure of the column ends during the test. A schematic view of the cross-sectional dimensions of short CFDST columns is presented in Fig. 2. Premix concrete was used to construct the columns. Two different batches of concrete mixes were used. The hollow steel tubes were filled with concrete in layers and the compaction of concrete was conducted by a vibrator. The test parameters included loading application (concentric or eccentric loading), load eccentricity ratio (e / B_o) with B_o being the width of the outer steel tube, diameter-to-thickness ratios of the internal tube (D_i / t_i) and steel yield strength. The length of the CFDST columns was three times the width of the external tubes to prevent the overall column buckling. The geometric and material properties of all specimens are provided in Table 1.

2.2. Material properties

The material properties of steel tubes were obtained by conducting tensile coupon tests in accordance with AS 1391 [31]. The average steel yield strengths of steel specimens presented in Table 2 were calculated from the test results of two coupon specimens for each tube. The yield strengths of the external steel tubes of 125×125×4.0 mm and 150×150×5.0 mm were measured as 360 MPa and 378 MPa, respectively. The yield strengths of the inner steel tubes varied from 345 MPa to 412 MPa. The stress-strain curves for steel material obtained from tensile coupon tests are presented in Fig. 3.

The material properties of concrete were determined by undertaking compression tests on 100×200 mm concrete cylinders. The concrete compressive strength was averaged from the test results of 42 concrete cylinders tested from the start to the end of the experimental program. The average compressive strength of the specimens in Group G1 and G2 was measured as 19.1

MPa while for the specimens in Group G3 and G4 it was measured as 20.6 MPa. The reason for the use of the low concrete compressive strength was because all column specimens were originally designed to be tested using the compression testing machine with a capacity of 2000 kN at Victoria University, Australia. However, due to the failure of the machine, all column specimens were tested at the University of Wollongong.

2.3. Test setup and instrumentation

The typical test setup of CFDST short columns is shown in Fig. 4. For CFDST stub columns under concentric loading, the axial load was applied to the concrete and steel simultaneously as illustrated in Fig. 4(a). The column ends were grinded using a concrete grinder prior to placing the column on the compression testing machine to ensure flat and smooth surface ends in order to obtain uniform load distribution. For short CFDST columns under eccentric loading, they were tested under pin-ended conditions by applying the compressive load on the loading heads attached to the column ends as illustrated in Fig. 4(b). The loading heads were designed by Hadi and Widiarsa [32] that consisted of a 50 mm thick square steel cap called the adaptor plate and a 25 mm thick bottom steel plate with a ball joint. The load generated by the compression testing machine was transferred through the bottom plate and ball joint to the adaptor plate with designed eccentricities.

Two strain gauges were attached to the column mid-height (one in each of the adjacent sides of the square column) to capture the axial and transverse strains under concentric loading as illustrated in Fig. 4(a). For columns under eccentric loading, two strain gauges were attached to the columns mid-height (one at each of the compression and tension sides) to capture the axial strain only. The axial shortening of square CFDST columns was averaged from the

readings of the two linear variable differential transducers (LVDTs) attached to the two opposite corners of the machine. For columns under eccentric loading, one additional laser triangulation was utilized to capture the column mid-height deflection as shown in Fig. 4(b).

All CFDST columns were tested to failure using the Denison 5000 kN compression testing machine at the structure laboratory in the School of Civil, Mining and Environmental Engineering at the University of Wollongong, Australia. The specimen was initially preloaded to 100 kN using the force-controlled mode to prevent any movement between the specimen and loading head of the testing machine, and then unloaded to 20 kN before starting recording the data. The column was loaded gradually with a displacement rate of 0.8 mm/min until the failure occurred. The test process was stopped when the external steel tube underwent significant local buckling or the maximum axial shortening reached to 30 mm. The readings of the LVDTs, strain gauges, laser triangulation and applied load were recorded using a data logger.

3. Test results and discussions

3.1. Failure modes and behavior of columns under compression

The short CFDST square columns failed by the significant unilateral local buckling of the flanges and webs of the external square steel tubes. The failure patterns of the CFDST short columns with square sections loaded concentrically are shown in Fig. 5. The stiffeners effectively prevented the steel tube ends from the premature failure due to local buckling during the test. Consequently, the outer steel tube generally buckled at the position about one third measured from the column top or bottom end. The outer steel tube of Column SC1 split at the corners where the adjacent tube walls buckled locally outward as shown in Fig. 5. Figure 6

presents the section view of Column SC1. It can be observed that the crushing of the sandwiched concrete took place at the regions where the local buckling of the external steel tube occurred. As demonstrated in Fig. 6, the core-concrete did not crush because of the confinement offered by the internal circular steel tube.

The measured ultimate loads of CFDST columns loaded concentrically to failure are given in Table 1 while their axial load-shortening curves are depicted in Fig. 7. It would appear from Fig. 7 that short CFDST columns exhibit strain-hardening behavior and very good ductility because of the utilization of internal circular steel tubes. The columns can sustain large axial deformation without a significant strength degradation. The residual strengths of Columns SC1, SC6, SC11 and SC16 were measured as 93%, 96%, 99% and 97% of their corresponding ultimate axial strengths, respectively. For the identical external steel tube, increasing the thickness (t_i) of the internal steel tube improves the column ultimate load slightly. Columns SC1 and SC11, SC6 and SC16 had the same outer tube, however, the ultimate loads of Column SC11 and SC16 are higher than those of Columns SC1 and SC6 due to the increased steel areas. The strain distributions in specimens loaded concentrically were measured during the tests and are given in Fig. 8. Figure 8(a) shows the relationships of the axial load and axial strains as well as lateral strains. In Fig. 8(b), the relationships of the lateral strain (hoop strain) and axial strain are provided. It is seen that both the axial and lateral strains increased at a small rate at the initial state of the loading. This is attributed to the effect of the Poisson's ratio of concrete, which was smaller than that of steel at the initial stage. However, after a certain load, the lateral strain increased significantly as the load increased due to the rapid expansion of the concrete.

3.2. Failure modes and behavior of columns under eccentric loading

The failure of CFDST square beam-columns loaded eccentrically were caused by the unilateral local buckling of the compression flange and the two adjacent webs in the external steel tube, the crushing of sandwiched concrete at places where local buckling occurred and the significant bending of the beam-columns as illustrated in Fig. 9. It is observed from Fig. 10 that the sandwiched concrete was separated from the internal steel tube. Columns SC5 and SC15 were subjected to eccentric loads with a large eccentricity ratio of 0.32. These two columns failed shortly due to the significant damage of the column bottom end where the load was applied as depicted in Fig. 11. The section view of Column SC14 is given in Fig. 12. It can be seen that the sandwiched concrete crushed at the compression zone where the steel tube wall underwent local buckling.

The load-axial shortening curves of CFDST square columns loaded eccentrically are presented in Fig. 13. It would appear that increasing the loading eccentricity greatly decreases the axial stiffness and ultimate strengths of short columns. The measured column ultimate strengths are tabulated in Table 1. For columns in Group 1, increasing the loading eccentricity from 0 mm to 10 mm, 20 mm, 30 mm and 40 mm reduces its ultimate axial strength by 11.2%, 30.2%, 43.2% and 49.6%, respectively. However, for the identical external steel tube, the reduction in the ultimate strength due to the eccentric loading was generally higher for the columns with thicker inner tube. The columns in Group G3 had a similar external tube as Group G1, however, the reduction in the ultimate axial strength was estimated as 18.3%, 31%, 39.4% and 55.1% for increasing the loading eccentricity from 0 mm to 10 mm, 20 mm, 30 mm and 40 mm, respectively. The experimentally measured load-lateral deflection curves of CFDST columns are provided in Fig. 14. It is evident the initial bending stiffness of CFDST columns decreases as the loading eccentricity increases. Figure 15 demonstrates the experimental load-axial strain curves of CFDST columns subjected to various end eccentricities. It is observed from Fig. 15

that at the initial loading stage, the CFDST column was subjected to compression. However, as the load increased, the axial strain in one of the steel tube walls became negative, which implies that part of the column was under tension.

4. Numerical model based on fiber element formulation

4.1. The method of fiber analysis

The key aspect of designing square CFDST beam-columns is the calculation of the cross-section strength under eccentric loading. The axial load-moment interaction diagrams (strength envelopes) of composite columns are often used to evaluate the strengths of short and slender composite columns subjected to combined actions. A mathematical model underlying the theory of fiber analysis has been proposed for calculating the axial load-moment-curvature relationships and strength envelopes of rectangular CFST beam-columns by Liang [33, 34]. Fiber elements are used to mesh the column cross-section as shown in Fig. 16. A mesh generator developed by Persson and Strang [35] is employed to discretize the sandwiched concrete in the present study. The formulation assumes that after deformation the plane section remains plane, which implies that a linear strain distribution through the depth of the cross-section is achieved as illustrated in Fig. 16. This assumption ensures the strain compatibility of steel and concrete fibers in the cross-section in the loading history. The stress of each fiber is calculated from its corresponding strain by applying the uniaxial stress-strain laws of concrete and steel materials. The internal bending moment (M) as well as the axial force (P) are determined by integrating the stresses over the cross-section.

4.2. Modeling of local and post-local buckling

The unilateral local buckling of the flanges and webs of a thin-walled CFST square column loaded eccentrically may take place, which leads to a marked reduction in the column ultimate resistance [22, 24]. The longitudinal stresses on the steel flanges and webs of the CFST column loaded uniaxially are either non-uniform or uniform as discussed by Liang et al. [24]. Liang et al. [24] developed formulas for ascertaining the initial local buckling strengths of steel flanges and webs subjected to non-uniform compressive stresses in CFST rectangular columns. Their expressions are employed in the present mathematical model.

The gradual post-local buckling characteristics of the flanges and webs of a CFDST column loaded eccentrically are modeled by the principle of stress redistributions as shown in Fig. 17. The effective widths of the thin-walled steel tube walls subjected to stress gradients are calculated using the formulas developed by Liang et al. [24]. Their effective width expressions can be used for steel plates with clear width-to-thickness ratios (b/t) ranging from 30 and 100. After the initial local buckling took place, the plate ineffective width increased as the compressive load increased until the plate reached its strength of post-local buckling. The computational scheme for modeling the gradual post-local buckling of a square CFST column loaded eccentrically proposed by Liang [33] is utilized in the present mathematical model.

4.3. Modeling of axial load-moment strength interaction diagrams

An incremental-iterative computational procedure has been developed for quantifying the strength envelopes of short square CFDST beam-columns subjected to axial compression in addition to uniaxial bending. The ultimate axial load (P_o) of the column without bending moment is initially calculated by using the load-axial strain response analysis technique that accounts for post-local buckling influences [33]. For a given axial load (P_u), the curvature (ϕ

) of the cross-section is incrementally increased and the corresponding moment is calculated that satisfies the force equilibrium. The section ultimate bending resistance is taken as the maximum moment on the predicted moment-curvature curve. By increasing the axial load from zero to the maximum value (P_o) and calculating the corresponding ultimate bending resistance, a set of ultimate moments and axial loads can be determined, which are used to plot the strength envelope of the CFDST column. The computer flow chart for calculating the strength envelope of a short CFDST column is shown in Fig. 18.

In the analysis, the neutral axis depth (d_n) of the cross-section is adjusted iteratively until the force equilibrium condition is achieved. The inverse quadratic method [36] has been implemented in the computer algorithms to determine the neutral axis depth. In the computational method, three values are initialized to the neutral axis depth. The new neutral axis depth approaching the true value is calculated by means of executing the following equations:

$$d_{n,j+3} = d_{n,j+1} - r_{p,j+1}\left(\frac{A}{C}\right) \tag{1}$$

$$A = (r_{p,j})^2(d_{n,j+2} - d_{n,j+1}) + r_{p,j}r_{p,j+1}(d_{n,j+1} - d_{n,j+2}) + (r_{p,j+1} - r_{p,j+2})r_{p,j+2}(d_{n,j} - d_{n,j+1}) \tag{2}$$

$$C = (r_{p,j+1} - r_{p,j})(r_{p,j+2} - r_{p,j})(r_{p,j+2} - r_{p,j+1}) \tag{3}$$

where $r_p = P_u - P$ and j is the iteration number. The initial three values of neural axis depths are taken as $d_{n,1} = D_0$, $d_{n,2} = D_0/2$ and $d_{n,3} = \left(d_{n,1} + d_{n,2}\right)/2$. The iterative computational process is stopped when the convergence criterion of $\left|r_p\right| < \varepsilon_k$ is achieved, where ε_k is taken as 10^{-4}.

4.4. Material constitutive laws for steels

The external tube of a square CFDST column is subjected to biaxial stresses under compression. This results in the reduction of steel yield strength which is taken into account in the material laws for structural steel as illustrated in Fig. 19, where f_{sy} denotes the steel yield strength, ε_{sy} the yield strain, ε_{st} the strain at the onset of strain-hardening, f_{su} the tensile strength and ε_{su} the ultimate strain of steel. The rounded part of the stress-strain curve between $0.9\varepsilon_{sy}$ and ε_{st} is represented by the expression proposed by Liang [33] while formulas suggested by Mander [37] are used to determine the stresses after the strain hardening occurs. The strain ε_{st} and the ultimate strain ε_{su} are taken as 0.005 and 0.2, respectively.

4.5. Material constitutive laws for concrete

The internal and external tubes provide little confinement to the sandwiched concrete in a square CFDST column so that the sandwiched-concrete is treated as unconfined concrete. However, the core concrete is confined by the internal circular steel tube in a square CFDST column and this confinement is recognized in the material stress-strain relations for core-concrete in the present study. The material constitutive models for sandwiched-concrete and core-concrete in rectangular CFDST columns have been validated against experimental data by Ahmed et al. [27]. The general stress-strain curves for both confined concrete and unconfined concrete are schematically illustrated in Fig. 20.

The ascending branch of the stress-strain curves are described by the following expressions suggested by Mander et al. [38]

$$\sigma_c = \frac{f_{cc}^{'}(\varepsilon_c / \varepsilon_{cc}^{'})\lambda}{(\varepsilon_c / \varepsilon_{cc}^{'})^{\lambda} + \lambda - 1} \qquad \text{for} \quad 0 \le \varepsilon_c \le \varepsilon_{cc}^{'} \tag{4}$$

$$\lambda = \frac{E_c \varepsilon_{cc}^{'}}{E_c \varepsilon_{cc}^{'} - f_{cc}^{'}} \tag{5}$$

where σ_c and ε_c represent the longitudinal concrete compressive stress and corresponding strain, respectively; $f_{cc}^{'}$ and $\varepsilon_{cc}^{'}$ the compressive strength and corresponding strain of confined concrete, respectively; E_c the concrete elastic modulus [12], which is taken as

$$E_c = 4400\sqrt{\gamma_c f_c'} \ \text{(MPa)} \tag{6}$$

where $\gamma_c = 1.85 D_c^{-0.135}$ stands for the reduction factor given by Liang [33], which considers the column size effect on the concrete compressive strength, and D_c is taken as $(B_o - 2t_o)$.

The maximum compressive strength as well as its corresponding strain of the core-concrete are calculated by

$$f_{cc}^{'} = \gamma_c f_c^{'} + 5.2\ (\gamma_c f_c^{'})^{0.91} \left(\frac{f_{rp}}{\gamma_c f_c^{'}}\right)^{a} \quad \text{where} \quad a = (\gamma_c f_c^{'})^{-0.06} \tag{7}$$

$$\varepsilon_{cc}^{'} = \varepsilon_c^{'} + 0.045 \left(\frac{f_{rp}}{\gamma_c f_c^{'}}\right)^{1.15} \tag{8}$$

$$\varepsilon_c^{'} = \frac{(\gamma_c f_c^{'})^{0.225}}{1000} \tag{9}$$

where f_{rp} stands for the lateral pressure on the core-concrete, which is computed by the following equation suggested by Liang and Fragomeni [39]:

$$f_{rp} = \begin{cases} 0.7(v_e - v_s)\dfrac{2t_i}{D_i - 2t_i} f_{syi} & \text{for } \dfrac{D_i}{t_i} \le 47 \\ (0.006241 - 0.0000357\dfrac{D_i}{t_i}) f_{syi} & \text{for } 47 < \dfrac{D_i}{t_i} \le 150 \end{cases} \quad (10)$$

in which v_e and v_s stand for the Poisson's ratios of the steel tube with and without concrete infill. In the numerical analysis, $v_s = 0.5$ and the v_e suggested by Tang et al. [40] are adopted. The equation formulated by Lim and Ozbakkaloglu [41] is used to describe the descending branch of the stress-strain responses of confined concrete as well as the unconfined one, and is expressed as

$$\sigma_c = f_{cc}^{'} - \frac{f_{cc}^{'} - f_{cr}}{\left[1 + \left(\dfrac{\varepsilon_c - \varepsilon_{cc}^{'}}{\varepsilon_{ci} - \varepsilon_{cc}^{'}}\right)^{-2}\right]} \quad \text{for} \quad \varepsilon_c > \varepsilon_{cc}^{'} \quad (11)$$

in which f_{cr} denotes the residual strength of concrete and ε_{ci} the strain at the inflection point. The expressions suggested by Lim and Ozbakkaloglu [41] are used to determine f_{cr} for the core concrete while f_{cr} is equal to $\beta_c f_c^{'}$ for the sandwiched-concrete. By analyzing the available test data, Ahmed et al. [27] proposed β_c as

$$\beta_c = \begin{cases} 1 & \text{for } 0 \le \dfrac{B_o}{t_o} \le 24 \\ 1 - \dfrac{1}{15}\left(\dfrac{B_o}{t_o} - 24\right) & \text{for } 24 < \dfrac{B_o}{t_o} \le 33 \\ 0.000062\left(\dfrac{B_o}{t_o}\right)^2 - 0.011225\left(\dfrac{B_o}{t_o}\right) + 0.705288 & \text{for } 33 < \dfrac{B_o}{t_o} \le 100 \end{cases} \quad (12)$$

The strain (ε_{ci}) at the inflection point is specified as 0.007 for the sandwiched-concrete. The equation given by Lim and Ozbakkaloglu [41] is employed to calculate ε_{ci} for the core-concrete, taking into account the column size effect [27].

The stress-strain curves for concrete under tension is illustrated in Fig. 20, where the tensile strength is equal to $0.6\sqrt{\gamma_c f_c'}$ and the ultimate tensile strain is taken as ten times the strain at cracking.

4.6. Curvature ductility index

The curvature ductility of a CFDST column in bending is expressed by the following curvature ductility indicator:

$$PI_{cd} = \frac{\phi_u}{\phi_y} \quad (13)$$

where ϕ_u represents the curvature of the CFDST column when the moment reduces to 90% of its ultimate moment capacity in the post-peak range or the ultimate curvature where column shows ascending moment-curvature relationships. The yield curvature (ϕ_y) is taken as

$\phi_{0.75} / 0.75$, where $\phi_{0.75}$ stands for the curvature when moment attains 75% of the column ultimate moment capacity.

5. Experimental verification

The mathematical modeling technique developed is validated by comparing the simulated strength envelopes with experimentally measured data in Fig. 21. The experimental ultimate moments were calculated as $M_{u,\exp} = P_{u,\exp} \times e$, where $P_{u,\exp}$ denotes the ultimate axial load obtained from experiments provided in Table 1 and *e* stands for the loading eccentricity. In the moment-curvature analysis of each CFDST column, the ultimate concrete strain was taken as the concrete strain corresponding to the column ultimate axial load. It can be observed from Fig. 21 that the agreement between experimental results and numerical predictions is generally good. The ultimate moments of Specimens SC2 and SC7 obtained from the experiments are slightly higher than the computed results. The cause for this is likely due to the fact that the actual concrete strengths in the tested specimens were unknown and the average concrete strength was specified in the nonlinear analyses. As shown in Fig. 21, the experimental ultimate bending resistances of Specimens SC4, SC5 and SC15 are considerably lower than the predicted values. This is because Specimens SC4, SC5 and SC15 with large loading eccentricities failed prematurely by the damage of the column ends under the applied load as shown in Figs. 9 and 11. For columns subjected to a large loading eccentricity, it is suggested for future tests that a cantilever should be rigidly connected to the column ends to prevent the premature failure of the column ends. The limitation of the proposed numerical model is that it does not predict the premature failure of the loading heads.

6. Parametric study

The computer simulation program developed was used to determine the axial load-moment-curvature relationships and strength envelopes of square short CFDST columns with various width-to-thickness (B_o / t_o) ratios of the external tube, the diameter-to-thickness (D_i / t_i) ratio of the internal tube, concrete strength ($f_c^{'}$), steel yield strength (f_{sy}), axial load ratio (P_u / P_o) and local buckling effects. The details of the reference CFDST column are as follows: $B_o = 500$ mm, $t_o = 10$ mm, $D_i = 250$ mm, $t_i = 5$ mm, $f_{syo} = f_{syi} = 350$ MPa, $E_s = 200$ GPa, $f_{co}^{'} = f_{ci}^{'} = 40$ MPa.

6.1. Effects of B_o / t_o ratio

The influences of the B_o / t_o ratio of the external square tube on the structural behavior of CFDST columns were examined by using the computational technique. The thickness of the reference column was varied to give the B_o / t_o ratios of 30, 50, 75 and 100 while the other parameters were unchanged. Figure 22 presents the moment-curvature responses of the CFDST columns having various B_o / t_o ratios under a constant axial load (P_u), which was taken as 60% of the pure ultimate axial load of the column with the B_o / t_o ratio of 100. It is clearly shown that increasing the B_o / t_o ratio remarkably reduces the column initial bending stiffness and ultimate moment capacity. This is due to the reduction in the thickness and area of the steel tube and because of local buckling. The reduction in the ultimate moment capacity was calculated as 66.9% by changing the B_o / t_o ratio from 30 to 100. The curvature ductility of CFDST columns also decreases as the B_o / t_o ratio increases. When increasing the B_o / t_o ratio

from 30 to 50, 75 and 100, the curvature ductility index decreases from 4.62 to 3.75, 3.03 and 2.78, respectively. Furthermore, increasing the B_o / t_o ratio greatly reduces the pure ultimate axial load (P_o) and pure ultimate moment (M_o) of the CFDST columns as can be seen from the strength envelopes presented in Fig. 23. However, the B_o / t_o ratio has the most prominent influence on the pure ultimate bending resistance than on the pure ultimate axial load (P_o). Changing the B_o / t_o ratio from 30 to 100 reduces the pure ultimate axial load by 39.0% and the pure ultimate moment by 62.1%, respectively.

6.2. Effects of D_i / t_i ratio

The computer simulation program was employed to ascertain the significance of the D_i / t_i ratio on the responses of the CFDST columns. The D_i / t_i ratios of 20, 30, 40 and 50 were obtained by altering the thickness t_i of the internal tube only. Figure 24 presents the influences of the D_i / t_i ratio on the axial load-moment-curvature behavior of CFDST columns under the axial load of $P_u = 9388$ kN. It would appear that the D_i / t_i ratio has a minor influence on the initial bending stiffness of CFDST columns. However, increasing the D_i / t_i ratio considerably reduces the column ultimate bending resistance. The column ultimate moment is reduced by 8.9%, 14.3% and 19.3%, respectively, by changing the D_i / t_i ratio from 20 to 30, 40 and 50. Varying the D_i / t_i ratio from 20 to 50 decreases the curvature ductility index from 5.46 to 3.35. The strength envelopes of CFDST columns as a function of D_i / t_i ratios are given in Fig. 25. It is seen that the D_i / t_i ratio has a moderate influence on the column ultimate axial and bending resistances. When the D_i / t_i ratio is increased from 20 to 50, the column pure ultimate axial and bending strengths are found to reduce by 11% and 8.5%, respectively. This is because

increasing the D_i / t_i ratio reduces the confinement exerted on the core-concrete, which reduces the column ultimate resistances.

6.3. Effects of steel yield strength

The sensitivities of the moment-curvature and interaction behavior of CFDST columns to the steel yield strength f_{sy} were investigated by varying f_{sy} from 250 MPa to 690 MPa. The predicted moment-curvature relationships of CFDST columns subjected to the same axial load of $P_u = 9388$ kN have been plotted in Fig. 26. It is discovered that the initial bending stiffness and ultimate bending resistance of CFDST columns are markedly improved by using steel tube with higher yield strength. When altering the yield strength from 250 MPa to 350 MPa, 480 MPa and 690 MPa, the column bending resistance increases by 52.1%, 116.0%, and 220.1%, respectively. As shown in Fig. 26, the column curvature ductility also improves as the yield strength increases. The calculated column curvature ductility indices with yield strengths of 250 MPa, 350 MPa and 480 MPa are 2.69, 3.35 and 4.34, respectively. Figure 27 gives the strength envelopes of CFDST columns, which have been plotted by demonstrating the effect of steel yield strength. It is illustrated that the use of higher strength steel tube remarkably improves the ultimate bending and axial resistances of CFDST columns. The numerical results show that changing the yield strength from 250 MPa to 690 MPa leads to 70.5% improvement in the pure ultimate axial load and 133.2% increase in the pure ultimate bending resistance of the column.

6.4. Effects of concrete strength

Fiber analyses on CFDST short columns constructed by concrete with different compressive strengths were performed to ascertain the effects of concrete strength on their moment-

curvature and interaction strength characteristics. The CFDST columns were made of concrete with strengths ranging from 40 MPa to 100 MPa. The simulated moment-curvatures curves for the CFDST columns under a constant load of $P_u = 9388$ kN are provided in Fig. 28. The initial bending stiffness and ultimate bending resistance of CFDST columns are shown to considerably improve by using higher strength concrete. As a result of changing the concrete strength from 40 MPa to 100 MPa, the column ultimate bending resistance increases by 102.3%. However, using higher strength concrete in CFDST columns decreases their curvature ductility. The column with 100 MPa concrete has a curvature ductility index of 2.9 while the column with 40 MPa concrete has a value of 3.35. Figure 29 shows the complete axial load-bending resistance curves for CFDST columns with different concrete strengths. It is confirmed that using higher strength concrete improves both the ultimate bending and axial strengths of CFDST columns. However, the effect of concrete strength on the column pure ultimate axial load is more prominent than on its pure bending resistance. When the concrete strength is changed from 40 MPa to 100 MPa, the increase in the pure ultimate axial load and pure ultimate bending resistance is 75.8% and 12.9%, respectively.

6.5. Effects of local buckling

The local buckling effects on the axial load-moment-curvature and interaction responses of axial load and moment in the CFDST columns were ascertained by means of using the computational model proposed. The nonlinear analyses on the reference column with a B_o / t_o ratio of 100 were undertaken by ignoring and including local buckling, respectively. The local buckling effect on the moment-curvature behavior of the CFDST column under the axial load of $P_u = 7351$ kN is demonstrated in Fig. 30. It is evident that the local buckling of the outer steel tube markedly reduces the column initial bending stiffness, ultimate bending resistance

and curvature ductility. If the tube local buckling was not included in the analysis, the column ultimate bending resistance is overestimated by 23.6%. Figure 31 illustrates the local buckling influence on the complete strength envelopes. It is confirmed that the interaction strengths of the CFDST column are markedly reduced by the outward local buckling. The column ultimate axial capacity and pure bending resistance are overestimated by 7.4% and 9.5%, respectively by ignoring the effect of local buckling.

6.6. Effects of axial load ratio

The significance of the axial load ratio (P_u / P_o) on the moment-curvature responses of CFDST beam-columns loaded eccentrically was examined by incorporating the axial load ratios from 0.2 to 0.8. The predicted moment-curvature responses have been plotted in Fig. 32. It is demonstrated that the influence of the axial load on the moment-curvature responses is remarkable. Increasing the axial load ratio significantly decreases the column initial bending stiffness, ultimate bending resistance and curvature ductility. The column ultimate bending resistance is found to reduce by 7.7%, 32.4% and 65.1% by increasing the P_u / P_o ratio from 0.2 to 0.4, 0.6 and 0.8, respectively. For the axial load ratios of 0.2, 0.4, 0.6 and 0.8, the curvature ductility indices were estimated as 4.61, 4.35, 3.35 and 2.72, respectively. This means that the column curvature ductility reduces by 6%, 27% and 41%, respectively, as the P_u / P_o ratio increases from 0.2 to 0.4, 0.6 and 0.8.

7. Conclusions

Experimental and numerical investigations on the structural performance of square CFDST stub columns loaded eccentrically have been presented in this paper. The experimental failure modes

and behavior of twenty square CFDST columns tested have been reported. A numerical model has been proposed for computing the axial load-moment-curvature relationships and interaction strengths of square CFDST stub columns incorporating local and post-local buckling. Efficient computational algorithms implementing the inverse quadratic method have been developed to obtain converged solutions. Good agreement between predictions and experimental data has been obtained. The computer model developed has been employed to perform a parametric study on the responses of CFDST columns considering important geometric and material parameters.

The following concluding remarks are given:

1. Square CFDST short columns loaded concentrically failed by the outward local buckling of the four walls of the external steel tube and the crushing of the sandwiched concrete. The CFDST columns tested under eccentric loading failed by the outward local buckling of the compression walls of the external steel tube, the crushing of the sandwiched-concrete and significant column bending. The core concrete in CFDST columns did not crush because the internal circular tube effectively confined the core-concrete.
2. Test results indicate that increasing the loading eccentricity markedly reduces the column ultimate loads as well as initial bending stiffness.
3. Numerical results demonstrate that the initial bending stiffness and ultimate axial and bending resistances of CFDST columns are remarkably decreased by increasing the B_o / t_o ratio and the axial load ratio but are only slightly decreased by increasing the D_i / t_i ratio.
4. Using higher yield strength tubes and high strength concrete appreciably improves the column initial bending stiffness, ultimate axial load and ultimate bending resistance, but

the concrete strength has a more pronounced effect on the pure ultimate load than on the pure bending strength.

5. The unilateral local buckling of the outer steel tube considerably reduces the ultimate axial and bending resistances of CFDST columns.

Square CFDST columns composed of an inner circular steel tube offer great benefits, such as high strength, high stiffness, high ductility and ease of connecting with steel beams, and can be used in high-rise composite buildings. To maximize their strengths and stiffness while maintaining good ductility, CFDST beam-columns should be designed with small B_o / t_o ratios, high strength steel tubes, suitable D_i / t_i ratios so that the inner tube effectively confines the concrete-core and high strength concrete within the inner tube.

Acknowledgements

The financial support provided by Victoria University and La Trobe University to conduct the experiments described in this paper is gratefully acknowledged. The authors would like to thank the technicians at both Victoria University and the University of Wollongong, Australia, particularly Mr. Ritchie McLean and Mr. Duncan Best at the University of Wollongong, Australia, for their assistance and help during the experiments.

References

[1] Peng YY, Tan KF, Yao Y. Mechanical properties of duplex steel tube high- strength concrete short columns under axial compression. J Wuhan University of Technol 2011;33 (2):105-109 (In Chinese).

[2] Liew JYR, Xiong DX. Ultra-High Strength Concrete Filled Composite Columns for Multi-Storey Building Construction. Adv Struct Eng 2012;15(9):1487-1503.

[3] Hassanein MF, Kharoob OF, Liang QQ. Behaviour of circular concrete-filled lean duplex stainless steel–carbon steel tubular short columns. Eng Struct 2013;56:83-94.

[4] Romero ML, Espinós A, Portolés J, Hospitaler A, Ibañez C. Slender double-tube ultra-high strength concrete-filled tubular columns under ambient temperature and fire. Eng Struct 2015;99:536-545.

[5] Wan CY, Zha XX. Nonlinear analysis and design of concrete-filled dual steel tubular columns under axial loading. Steel Compo Struct 2016;20(3):571-597.

[6] Ekmekyapar T, Al-Eliwi BJ. Concrete filled double circular steel tube (CFDCST) stub columns. Eng Struct 2017;135:68-80.

[7] Ibañez C, Romero ML, Espinós A, Portolés JM, Albero V. Ultra-high strength concrete on eccentrically loaded slender circular concrete-filled dual steel columns. Structures 2017;12:64-74.

[8] Romero ML, Ibañez C, Espinós A, Portolés J, Hospitaler A. Influence of ultra-high strength concrete on circular concrete-filled dual steel columns. Structures 2017;9:13-20.

[9] Xiong MX, Xiong DX, Liew JYR. Axial performance of short concrete filled steel tubes with high-and ultra-high-strength materials. Eng Struct 2017;136:494-510.

[10] Xiong MX, Xiong DX, Liew JYR. Behaviour of steel tubular members infilled with ultra high strength concrete. J Constr Steel Res 2017;138:168-183.

[11] Zheng Y, He C, Zheng L. Experimental and numerical investigation of circular double-tube concrete-filled stainless steel tubular columns under cyclic loading. Thin-Walled Struct 2018;132:151-166.

[12] Ahmed M, Liang QQ, Patel VI, Hadi MN. Numerical analysis of axially loaded circular high strength concrete-filled double steel tubular short columns. Thin-Walled Struct 2019;138:105-116.

[13] Pei WJ. Research on Mechanical Performance of Multibarrel Tube-Confined Concrete Columns. ME Thesis, Chang'an University, Xian, China, 2005 (in Chinese).

[14] Qian J, Zhang Y, Ji X, Cao W. Test and analysis of axial compressive behavior of short composite-sectioned high strength concrete filled steel tubular columns. J Build Struct 2011; 32(12):162-169 (in Chinese).

[15] Qian J, Zhang Y, Zhang W. Eccentric compressive behavior of high strength concrete filled double-tube short columns. J Tsinghua University, Sci Technol 2015;55(1):1-7 (in Chinese).

[16] Wang ZB, Tao Z, Yu Q. Axial compressive behaviour of concrete-filled double-tube stub columns with stiffeners. Thin-Walled Struct 2017;120:91-104.

[17] Zhong ST. Concrete Filled Steel Tubular Structures. Tsinghua University Press, Beijing, 2003 (in Chinese).

[18] Han LH. Concrete Filled Steel Tubular Structures: Theory and Practice. Science Press, Beijing, 1st Edition, 2000; Second Edition, 2007 (in Chinese).

[19] Sun YP, Kenji S. A comprehensive stress-strain model for high-strength concrete confined by circular transverse reinforcement. Proce of the Sixth Inter Conf on Steel-Concrete Compo Struct, Los Angeles, USA, 2000; 1067-1074.

[20] Tao Z, Wang, ZB, Yu Z.Finite element modelling of concrete-filled steel stub columns under axial compression. J Construct Steel Res 2013:89(10):121-131.

[21] Uy B. Local and post-local buckling of concrete filled steel welded box columns. J Constr Steel Res 1998;47(1-2):47-72.

[22] Liang QQ, Uy B. Theoretical study on the post-local buckling of steel plates in concrete-filled box columns. Comput Struct 2000;75(5):479-490.

[23] Liang QQ, Uy B, Liew JR. Nonlinear analysis of concrete-filled thin-walled steel box columns with local buckling effects. J Constr Steel Res 2006;62(6):581-591.

[24] Liang QQ, Uy B, Liew JYR. Local buckling of steel plates in concrete-filled thin-walled steel tubular beam–columns. J Constr Steel Res 2007;63(3):396-405.

[25] Huang Z, Li D, Uy B, Thai H-T, Hou C. Local and post-local buckling of fabricated high-strength steel and composite columns. J Constr Steel Res 2019;154:235-249.

[26] Song Y, Li J, Chen YY. Local and post-local buckling of normal/high strength steel sections with concrete infill. Thin-Walled Struct 2019;138:155-169.

[27] Ahmed M, Liang QQ, Patel VI, Hadi MNS. Nonlinear analysis of rectangular concrete-filled double steel tubular short columns incorporating local buckling. Eng Struct 2018; 175:13-26.

[28] Ahmed M, Liang QQ, Patel VI, Hadi MNS. Local-global interaction buckling of square high strength concrete-filled double steel tubular slender beam-columns. Thin-Walled Struct 2019; 143:106244..

[29] Ky VS, Tangaramvong S, Thepchatri T, Inealstic analysis for the post-collapse behavior of concrete encased steel composite columns under axial compression. Steel Compo Struct 2015; 19:1237-1258.

[30] Liu X, Bradford MA, Erkmen RE, Non-linear inealstic analysis of steel-concrete composite beams curved in-plan. Eng Struct 2013; 57: 484-492.

[31] AS 1391. Metallic Materials-Tensile Testing at Ambient Temperature. Standards Australia, Sydney, NSW, Australia, 2007.

[32] Hadi MNS, Widiarsa IBR. Axial and flexural performance of square RC columns wrapped with CFRP under eccentric loading. J Compos Constr ASCE 2012;16(6):640-649.

[33] Liang QQ. Performance-based analysis of concrete-filled steel tubular beam–columns, Part I: Theory and algorithms. J Constr Steel Res 2009;65 (2):363-372.

[34] Liang QQ. Performance-based analysis of concrete-filled steel tubular beam–columns, Part II: Verification and applications. J Constr Steel Res 2009;65(2):351-362.

[35] Persson P-O, Strang G. A simple mesh generator in MATLAB. SIAM Review 2004;46 (2):329-345.

[36] Epperson JF, An Introduction to Numeircal Methods and Analysis, Wiley-Interscience, 2007.

[37] Mander JB. Seismic design of bridge piers. Ph.D. Thesis, Department of Civil Engineering, University of Canterbury Christchurch, New Zealand,1983.

[38] Mander JB, Priestley MJ, Park R. Theoretical stress-strain model for confined concrete. J Struct Eng ASCE 1988;114(8):1804-1826.

[39] Liang QQ, Fragomeni S. Nonlinear analysis of circular concrete-filled steel tubular short columns under axial loading. J Constr Steel Res 2009;65 (12):2186-2196.

[40] Tang J, Hino S, Kuroda I, Ohta T. Modeling of stress-strain relationships for steel and concrete in concrete filled circular steel tubular columns. Steel Constr Eng, JSSC 1996;3(11):35-46.

[41] Lim JC, Ozbakkaloglu T. Stress–strain model for normal-and light-weight concretes under uniaxial and triaxial compression. Constr Build Mater 2014;71:492-509.

Figures and Tables

Table 1 Geometry and material properties of square CFDST short columns

Group	Column	Length L (mm)	Outer Tube		Inner Tube		f_c' (MPa)	e (mm)	e / B_o	$P_{u,\exp}$ (kN)
			$B_o \times B_o \times t_o$ (mm)	$\frac{B_o}{t_o}$	$D_i \times t_i$ (mm)	$\frac{D_i}{t_i}$				
G1	SC1	375	125×125×4.0	31.25	76.1×3.2	23.8	19.1	0	0	1269
	SC2	375	125×125×4.0	31.25	76.1×3.2	23.8	19.1	10	0.08	1127
	SC3	375	125×125×4.0	31.25	76.1×3.2	23.8	19.1	20	0.16	886
	SC4	375	125×125×4.0	31.25	76.1×3.2	23.8	19.1	30	0.24	721
	SC5	375	125×125×4.0	31.25	76.1×3.2	23.8	19.1	40	0.32	640
G2	SC6	450	150×150×5.0	30.00	88.9×3.2	27.8	19.1	0	0	1852
	SC7	450	150×150×5.0	30.00	88.9×3.2	27.8	19.1	10	0.07	1669
	SC8	450	150×150×5.0	30.00	88.9×3.2	27.8	19.1	20	0.13	1426
	SC9	450	150×150×5.0	30.00	88.9×3.2	27.8	19.1	30	0.20	1191
	SC10	450	150×150×5.0	30.00	88.9×3.2	27.8	19.1	35	0.23	1153
G3	SC11	375	125×125×4.0	31.25	76.1×3.6	21.1	20.6	0	0	1331
	SC12	375	125×125×4.0	31.25	76.1×3.6	21.1	20.6	10	0.08	1087
	SC13	375	125×125×4.0	31.25	76.1×3.6	21.1	20.6	20	0.16	918
	SC14	375	125×125×4.0	31.25	76.1×3.6	21.1	20.6	30	0.24	807
	SC15	375	125×125×4.0	31.25	76.1×3.6	21.1	20.6	40	0.32	597
G4	SC16	450	150×150×5.0	30.00	88.9×4.0	22.2	20.6	0	0	1865
	SC17	450	150×150×5.0	30.00	88.9×4.0	22.2	20.6	10	0.07	1624
	SC18	450	150×150×5.0	30.00	88.9×4.0	22.2	20.6	20	0.13	1377
	SC19	450	150×150×5.0	30.00	88.9×4.0	22.2	20.6	35	0.23	1171
	SC20	450	150×150×5.0	30.00	88.9×4.0	22.2	20.6	45	0.30	1033

Table 2 Material properties of steel tube obtained from tensile coupon tests.

Tube type	No.	Geometry of the tube (mm)	Yield strength, f_{sy} (MPa)	Ultimate strength, f_{su} (MPa)	Yield strain, ε_{sy}	Ultimate strain, ε_{su}	Elastic modulus, E_s (GPa)
Outer tube $B_o \times B_o \times t_o$	1	125×125×4.0	360	461	0.0053	0.25	203
	2	150×150×5.0	378	464	0.0033	0.23	201
Inner tube $D_i \times t_i$	1	76.1×3.2	400	458	0.0015	0.188	211
	2	88.9×3.2	412	471	0.0013	0.202	200
	3	76.1×3.6	353	398	0.0026	0.170	205
	4	88.9×4.0	345	372	0.0042	0.193	200

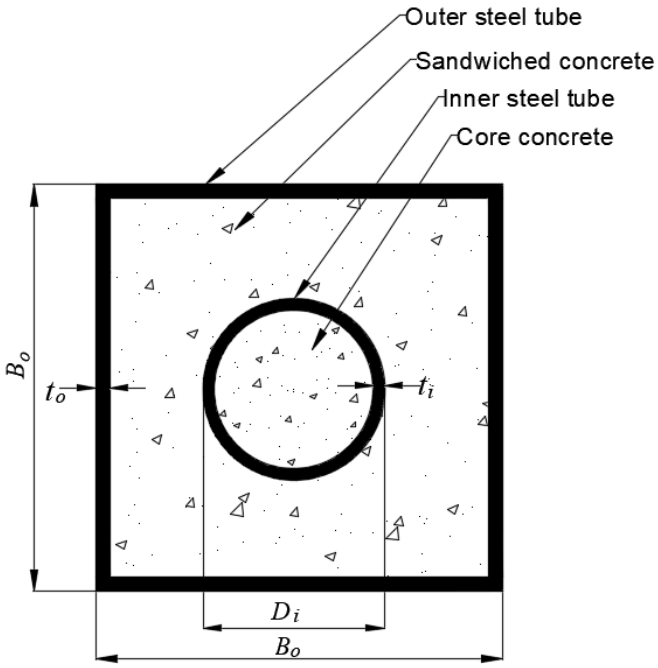

Fig. 1. Cross-section of square CFDST column with inner circular steel tube.

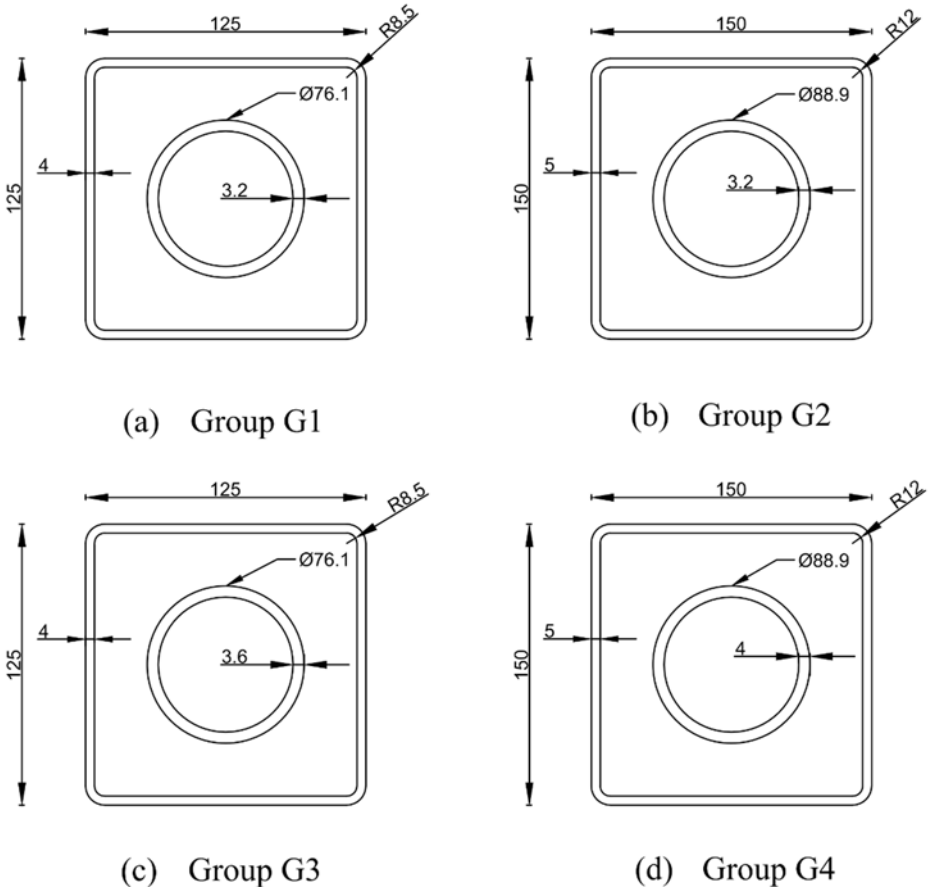

Fig. 2. Dimensions of test specimens.

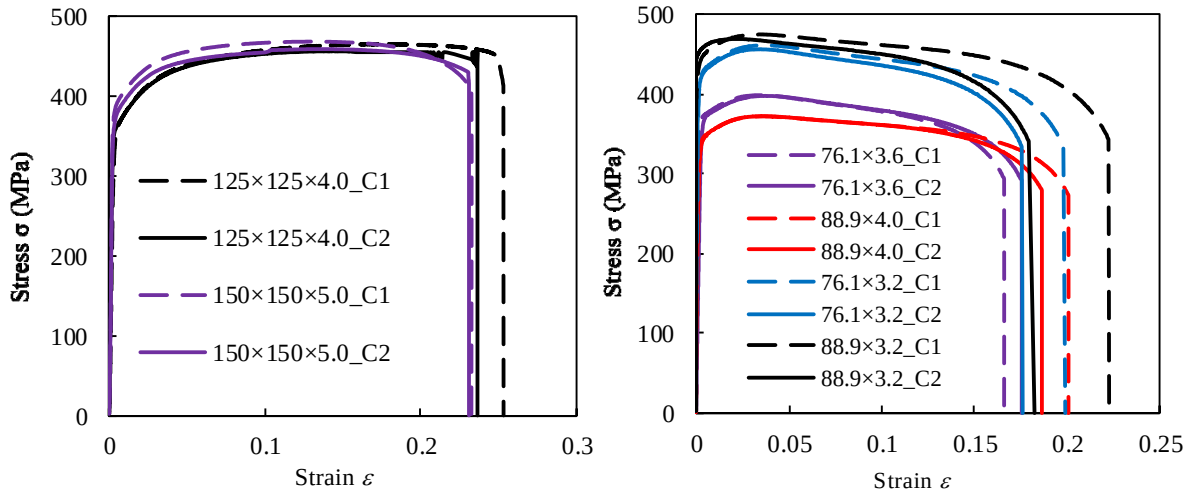

(a) Outer tube (b) Inner tube

Fig. 3. Measured stress-strain curves for steel tubes.

(a) Under concentric loading

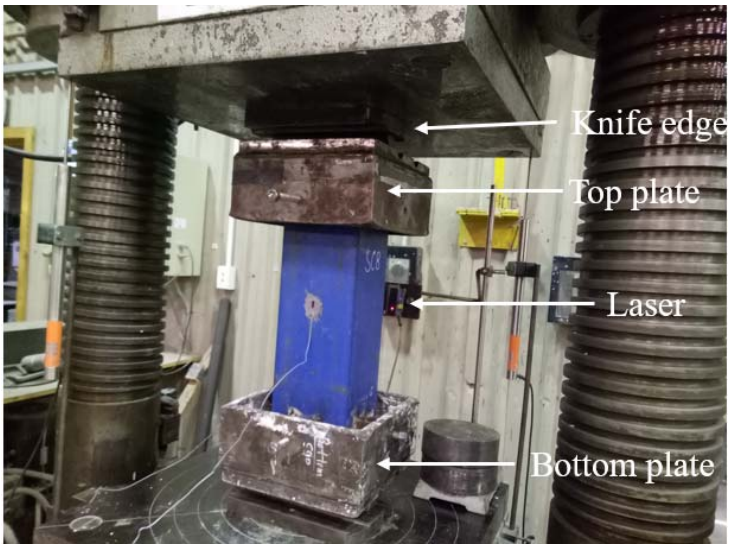

(b) Under eccentric loading

Fig. 4. Test setup of square CFDST short columns.

Fig. 5. Failure modes of square CFDST short columns under axial compression.

(a) (b)

Fig. 6. Section view of Specimen SC1.

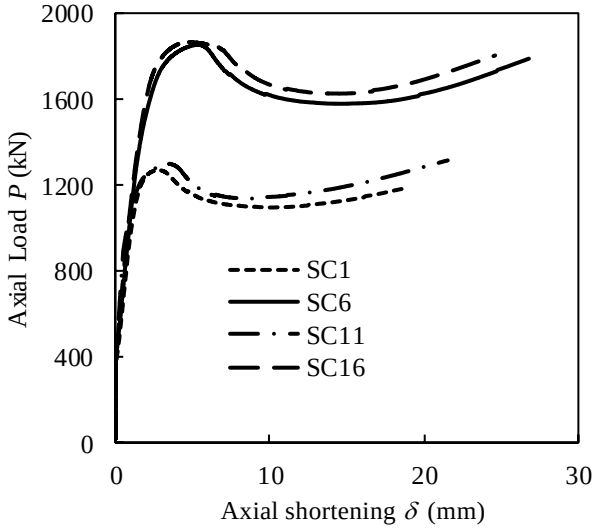

Fig. 7. Measured axial load-shortening curves of square CFDST short columns under axial compression.

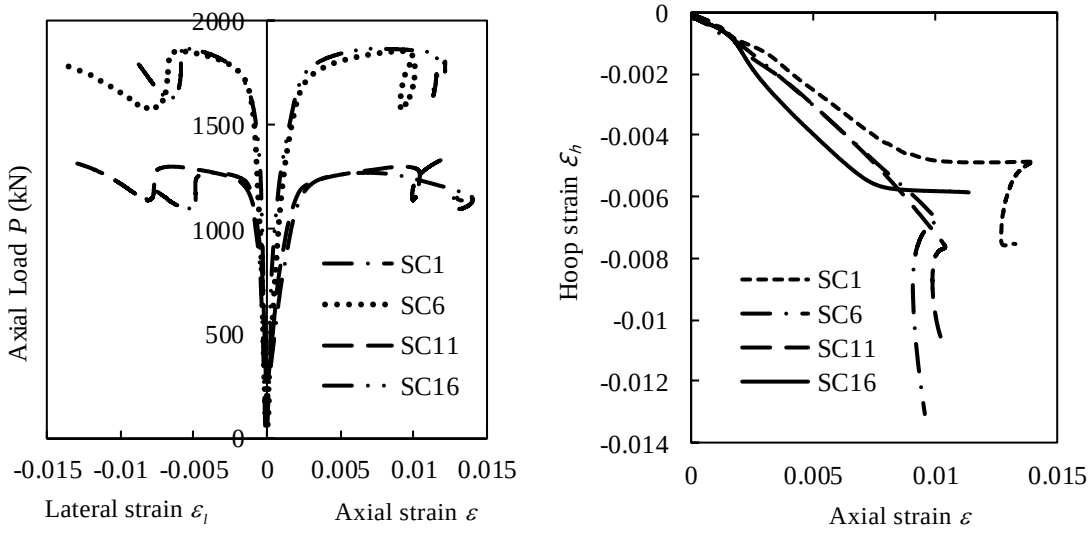

(a) (b)

Fig. 8. Strain distributions in square CFDST short columns under axial compression.

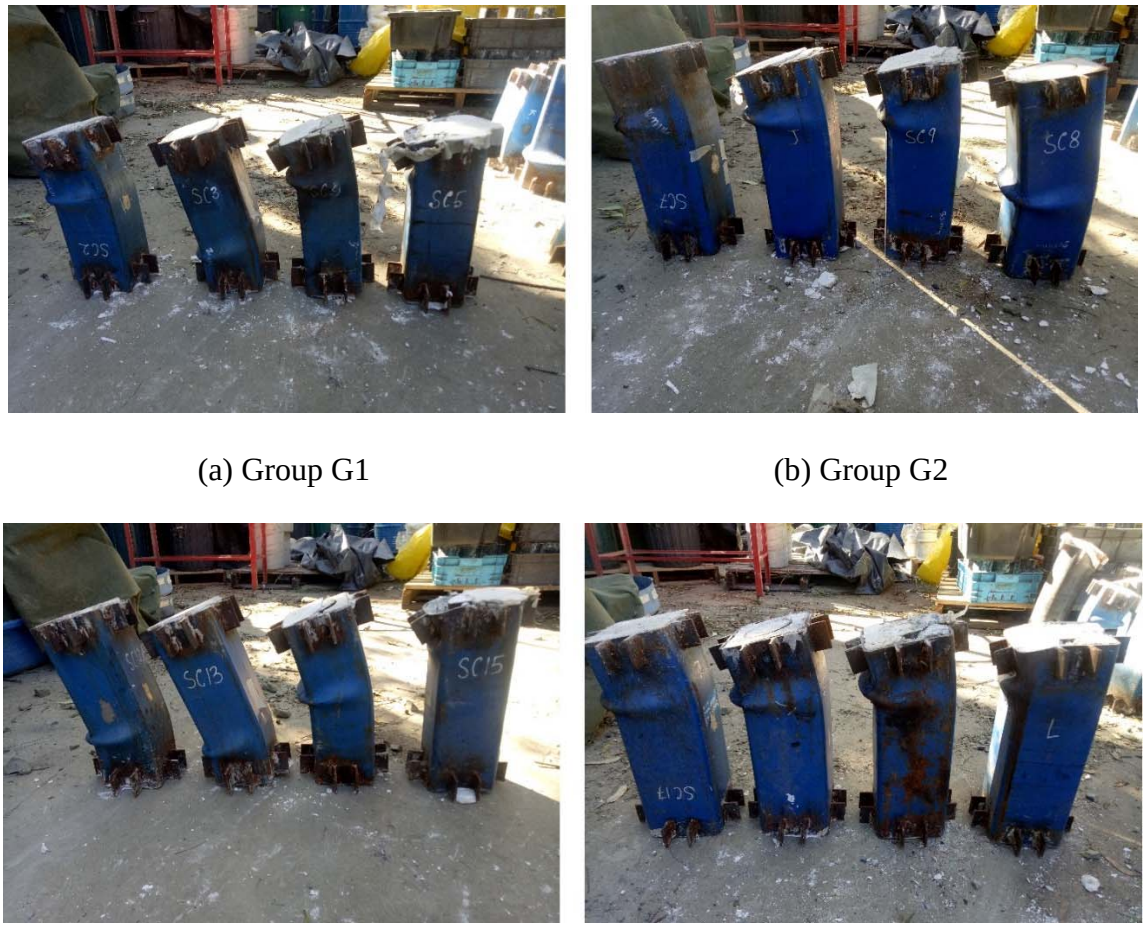

(a) Group G1 (b) Group G2

(c) Group G3 (d) Group G4

Fig. 9. Failure modes of square CFDST short columns under eccentric loading.

(a) Specimen SC8 (b) Specimen SC14

Fig. 10. Separation of sandwiched concrete and inner steel tube in Specimens SC8 and SC14.

(a) Specimen SC5 (b) Specimen SC15

Fig. 11. Failure modes of Specimens SC5 and SC15.

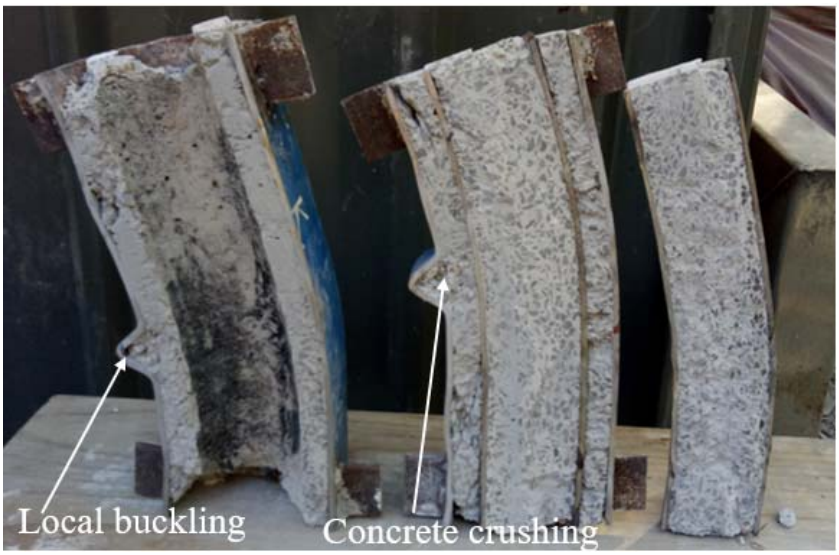

Fig. 12. Section view of Specimen SC14.

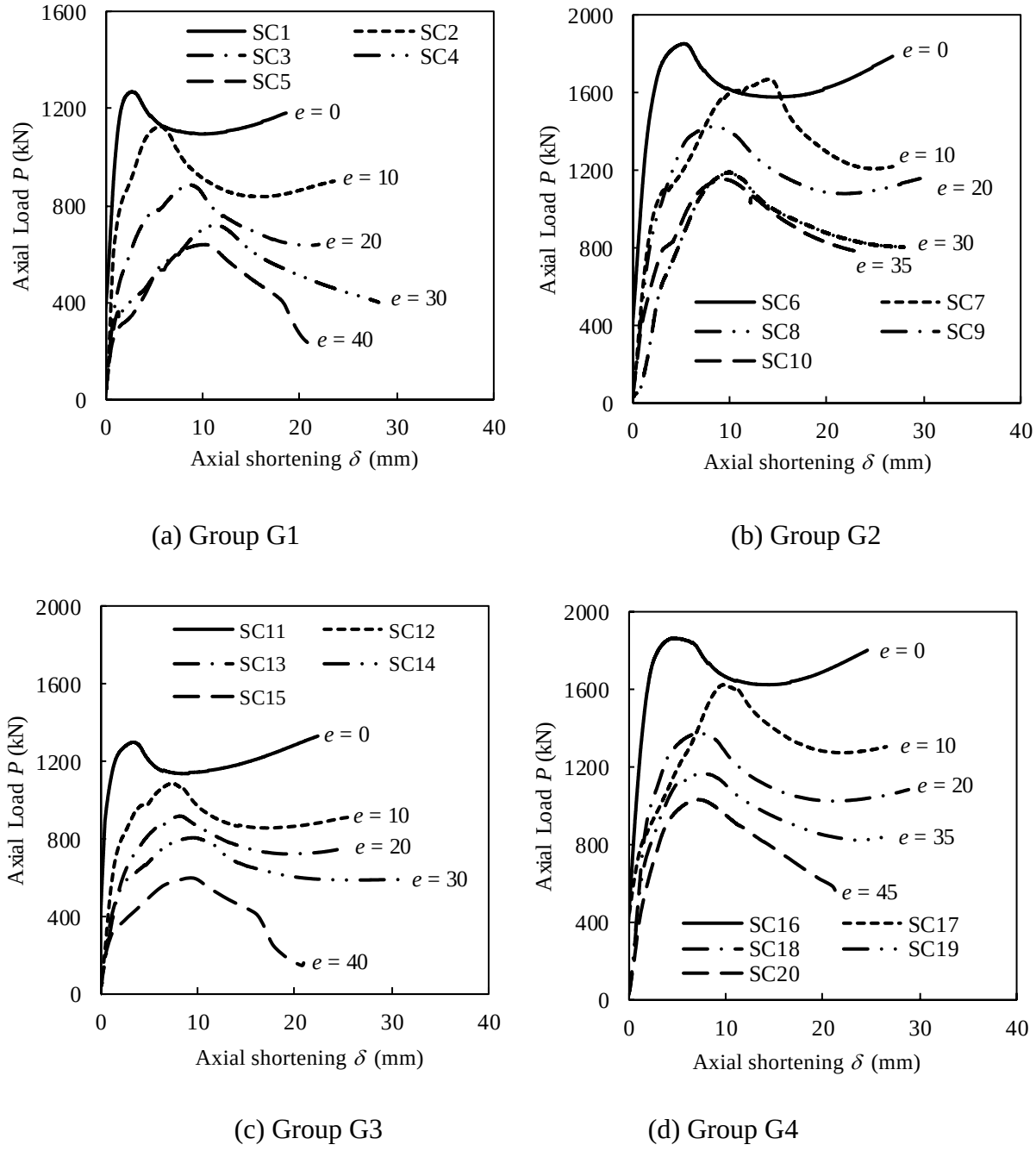

(a) Group G1

(b) Group G2

(c) Group G3

(d) Group G4

Fig. 13. Effects of loading eccentricity on the axial load-shortening curves of square CFDST columns.

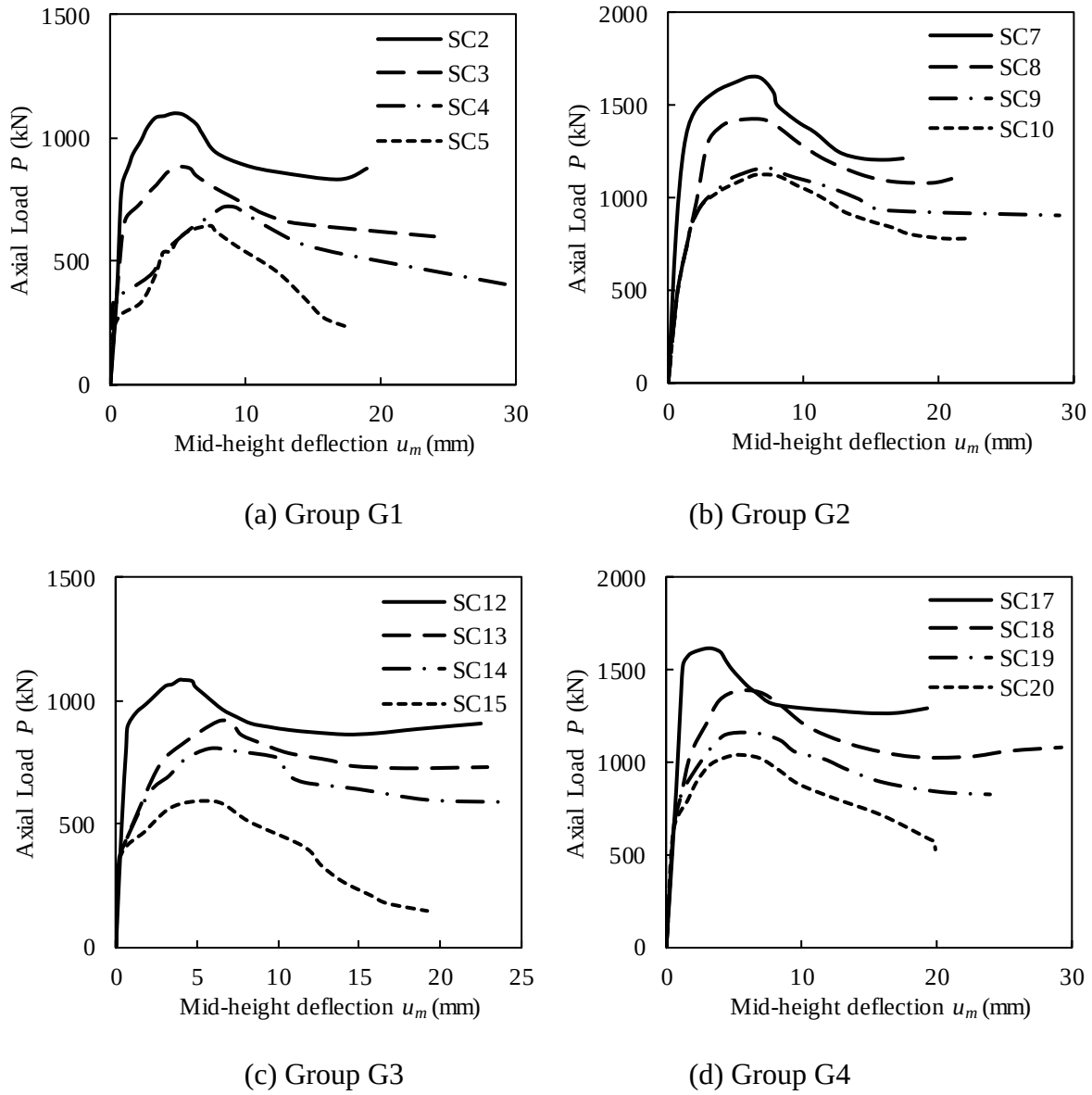

(a) Group G1 (b) Group G2

(c) Group G3 (d) Group G4

Fig. 14. Measured axial load-lateral deflection curves of square CFDST short columns under eccentric loading.

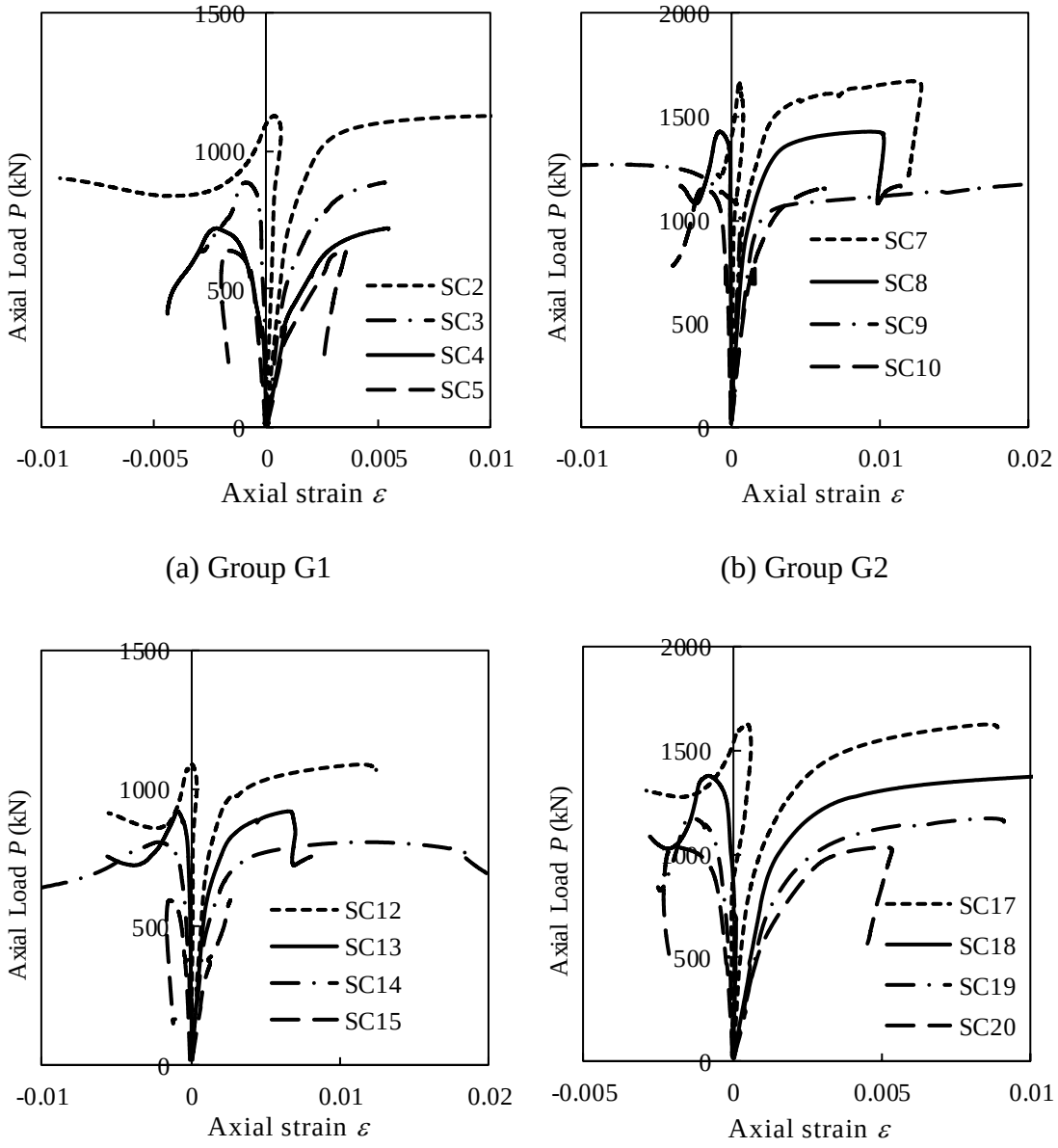

(a) Group G1 (b) Group G2

(c) Group G3 (d) Group G4

Fig. 15. Measured axial load-strain curves of square CFDST short columns under eccentric loading.

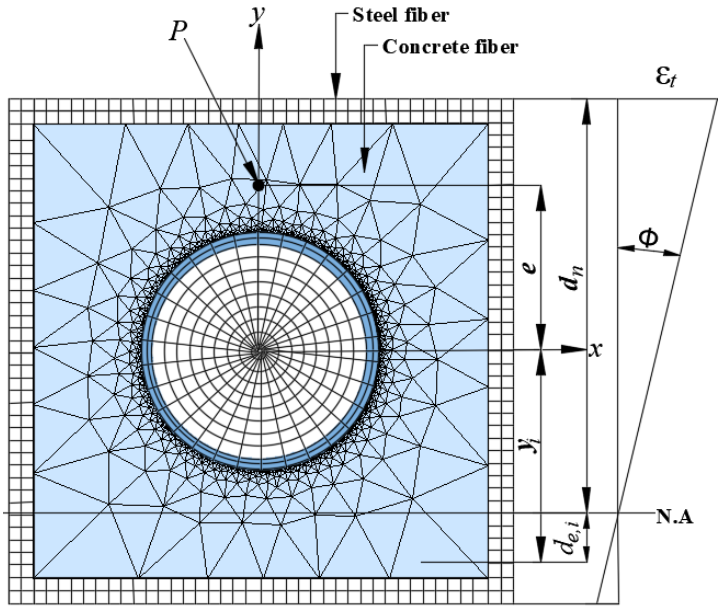

Fig. 16. Typical fiber discretization and strain distribution in the cross-section of square CFDST column.

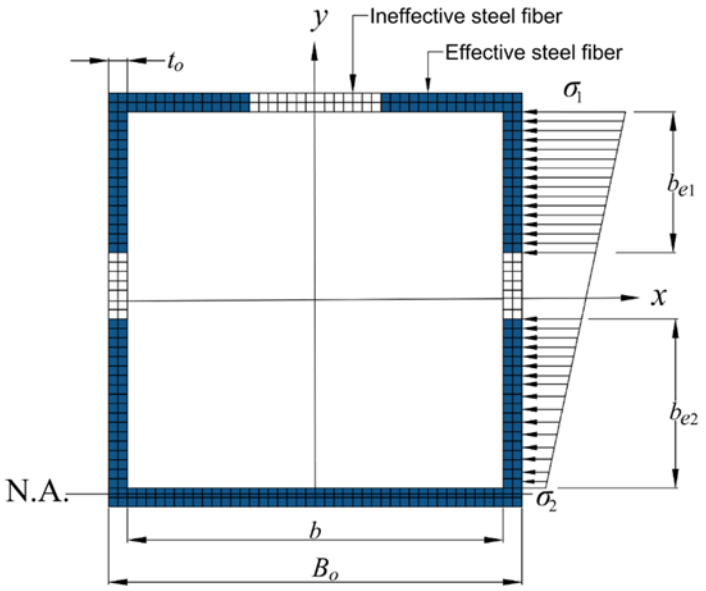

Fig. 17. Effective widths of the external steel tube of square CFDST column under eccentric loading.

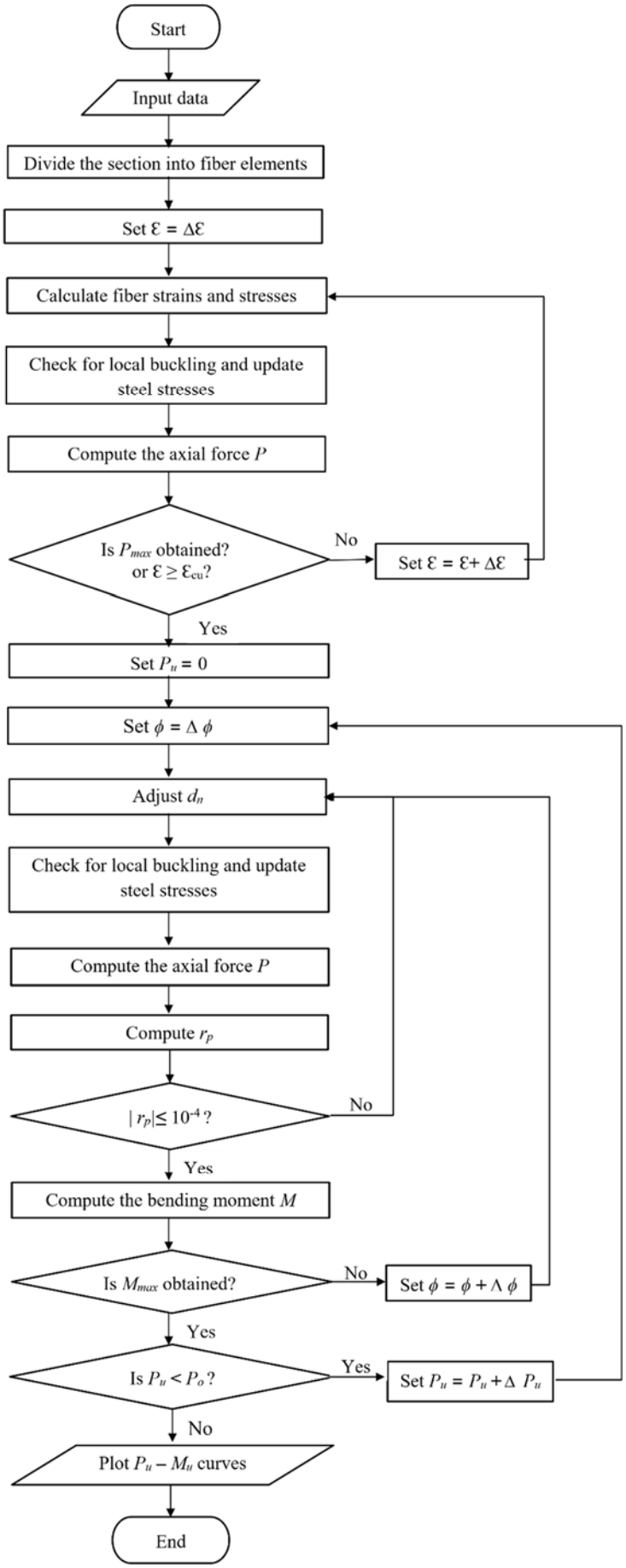

Fig. 18. Computer flowchart for calculating axial load-moment interaction curves.

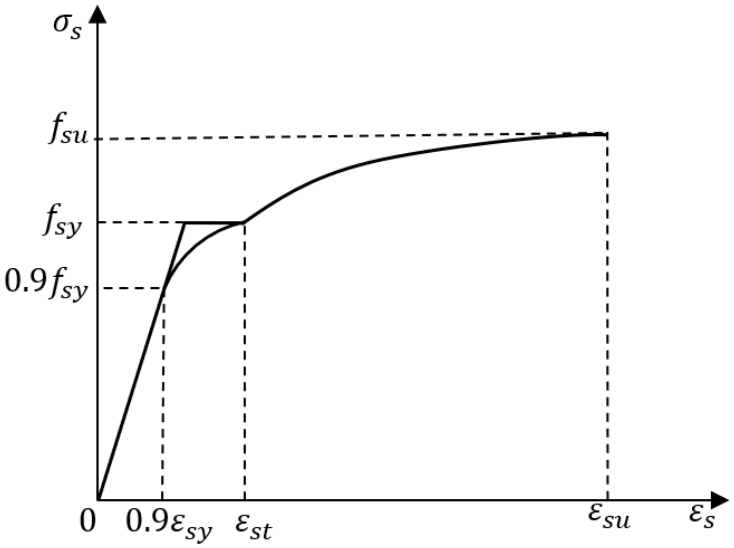

Fig. 19. Stress-strain curve for structural steels.

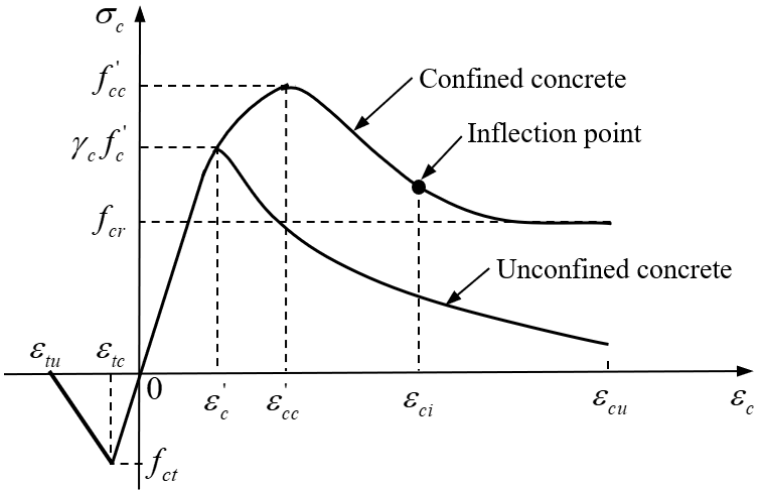

Fig. 20. Stress-strain curves for confined and unconfined concrete.

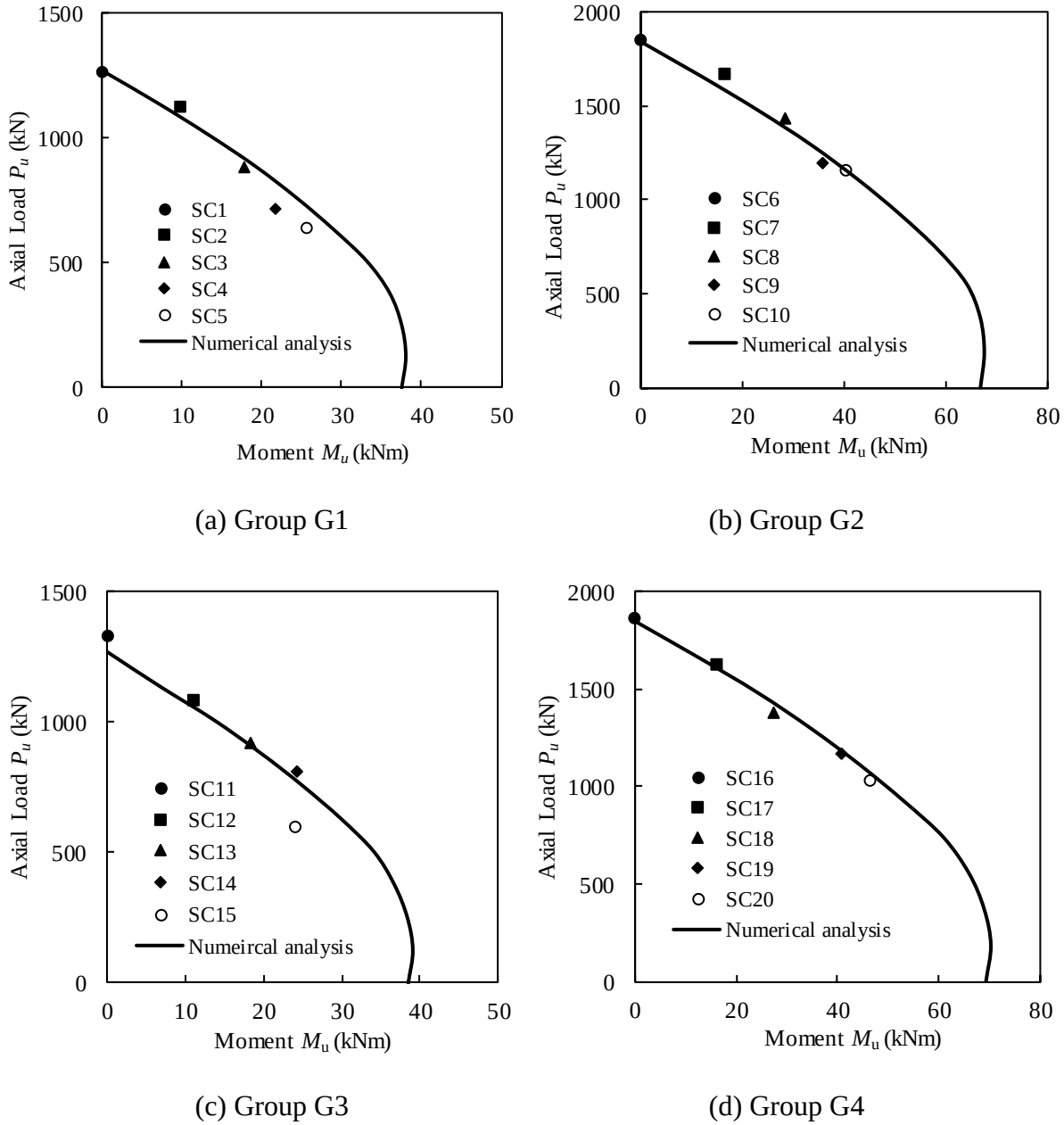

(a) Group G1

(b) Group G2

(c) Group G3

(d) Group G4

Fig. 21. Comparison of predicted strength envelopes of square CFDST columns with test results.

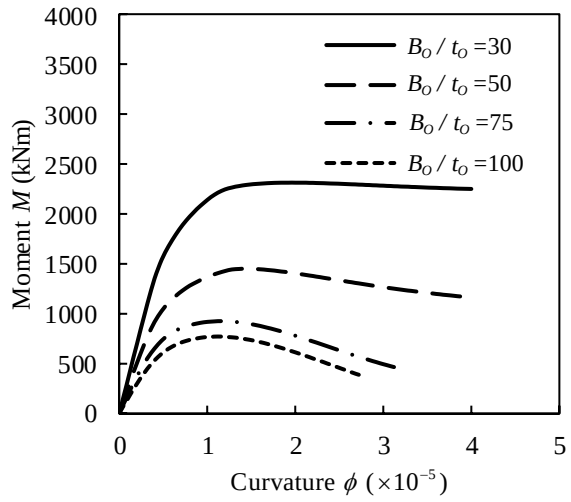

Fig. 22. Effects of B_o / t_o ratio on the moment-curvature curves of square CFDST columns.

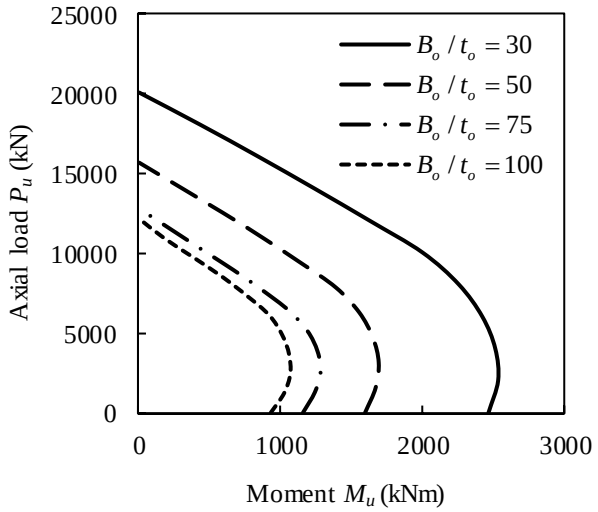

Fig. 23. Effects of B_o / t_o ratio on the strength envelopes of square CFDST columns.

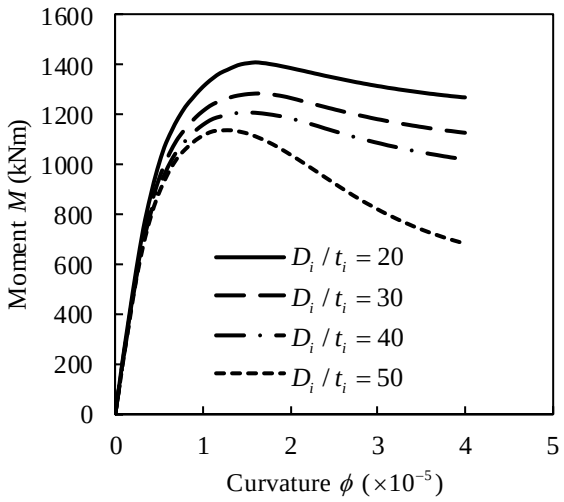

Fig. 24. Effects of D_i/t_i ratio on the moment-curvature curves of square CFDST columns.

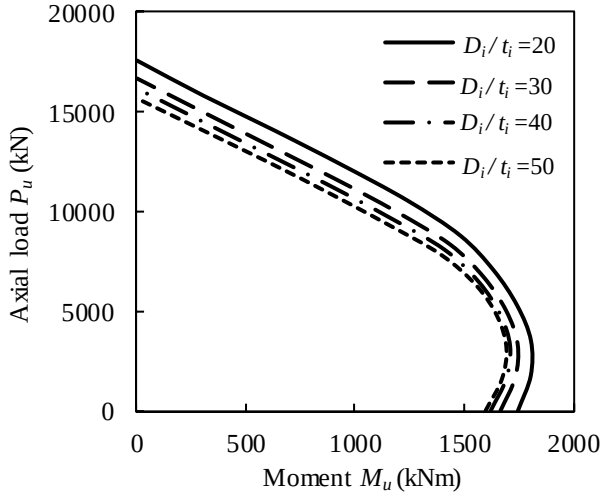

Fig. 25. Effects of D_i/t_i ratio on the strength envelopes of square CFDST columns.

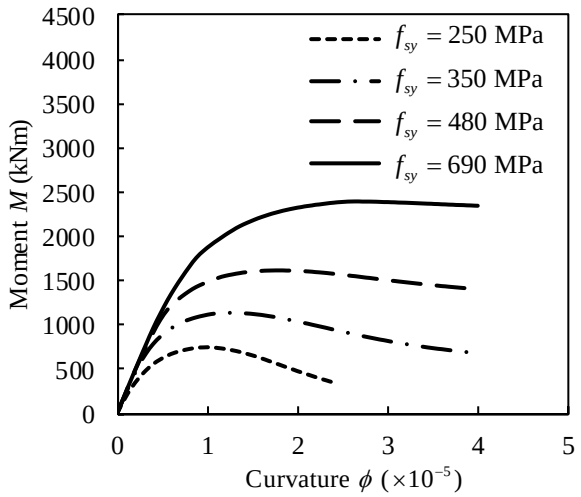

Fig. 26. Effects of steel yield strength on the moment-curvature curves of square CFDST columns.

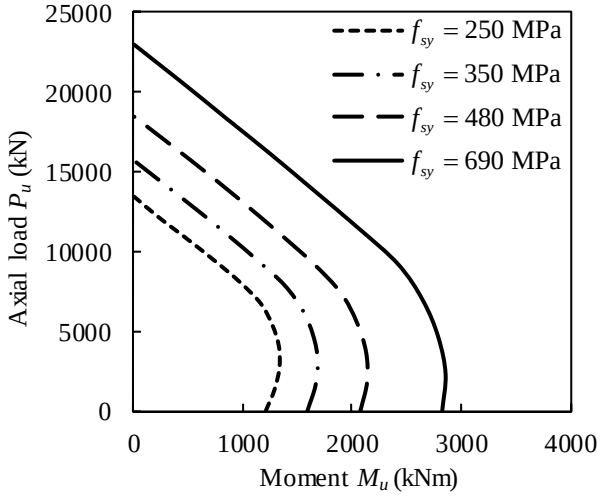

Fig. 27. Effects of steel yield strength on the strength envelopes of square CFDST columns.

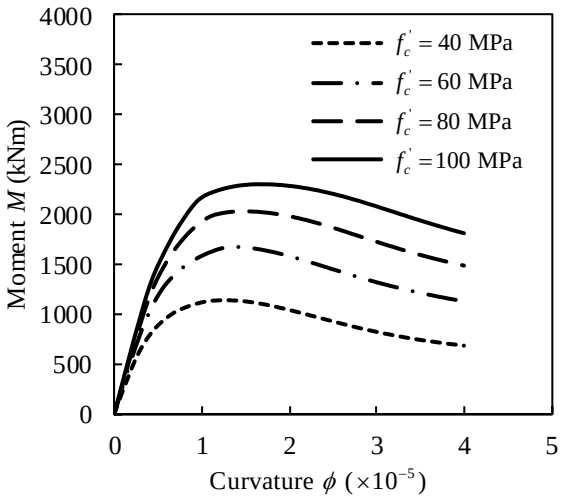

Fig. 28. Effects of concrete strength on the moment-curvature curves of square CFDST columns.

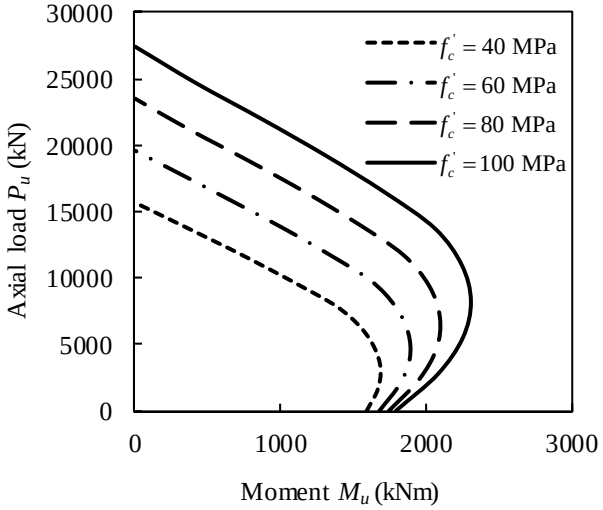

Fig. 29. Effects of concrete strength on the strength envelopes of square CFDST columns.

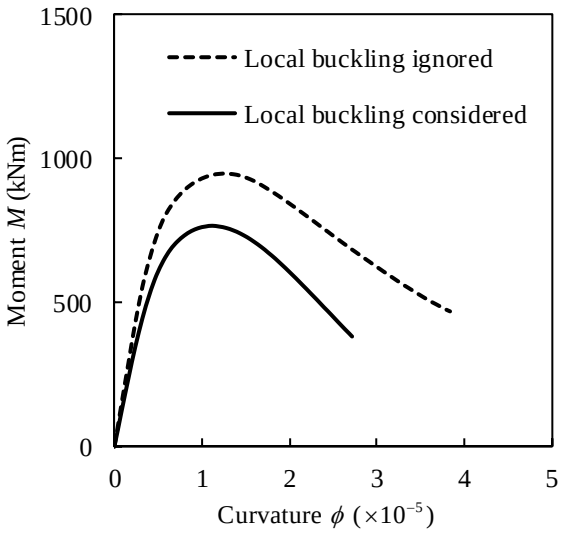

Fig. 30. Effects of the local buckling of the outer steel tube on the moment-curvature curves of square CFDST columns.

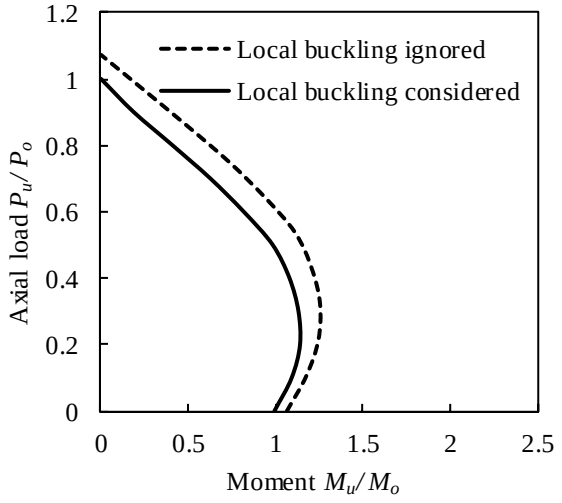

Fig. 31. Effects of the local buckling of the outer steel tube on the normalized strength envelopes of square CFDST columns.

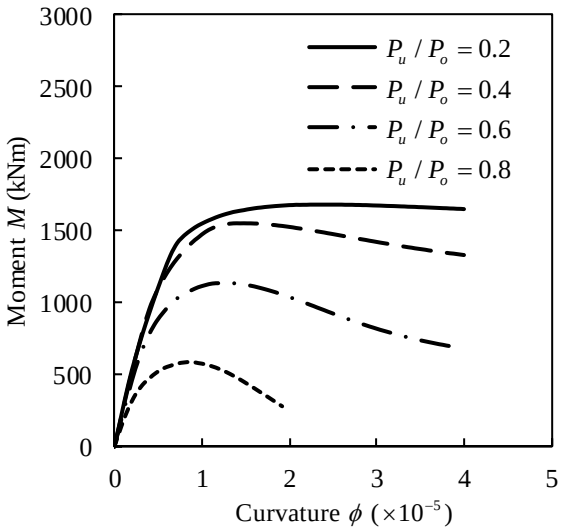

Fig. 32. Effects of axial load ratio on the moment-curvature curves of square CFDST columns.